Estimation of Variable-Speed-Drive Power Consumption From Harmonic Content

Kwangduk Douglas Lee, Steven B. Leeb, *Senior Member*, Leslie K. Norford, Peter R. Armstrong, Jack Holloway, *Student Member*, and Steven R. Shaw, *Senior Member*

***Abstract*—Nonintrusive load monitoring can be used to identify the operating schedule of individual loads strictly from measurements of an aggregate power signal. Unfortunately, certain classes of loads present a continuously varying power demand. The power demand of these loads can be difficult to separate from an aggregate measurement. Variable-speed drives (VSDs) are industrially important variable-demand loads that are difficult to track nonintrusively. This paper proposes a VSD power estimation method based on observed correlations between fundamental and higher harmonic spectral content in current. The technique can be generalized to any load with signature correlations in harmonic content, including many power electronic and electromechanical loads. The approach presented here expands the applicability and field reliability of nonintrusive load monitoring.**

***Index Terms*—Correlation, nonintrusive load monitoring, power estimation, variable speed drive.**

I. Introduction

A NONINTRUSIVE load monitor (NILM) can be used to estimate the operating schedule, power consumption, and impact on power quality associated with individual loads given only an aggregate measurement gathered from a central location [1]–[4]. The NILM samples raw voltage and current waveforms and computes harmonic content or *spectral envelopes* [5]. For loads that present a constant steady-state power demand, the NILM can easily compute energy consumption for individual loads by identifying their ON/OFF events and tracking their operating duration. The NILM is inexpensive to install, eases the problems of data collection and collation, and improves reliability by minimizing the number of sensors [6]. When a sensor system already exists, a NILM can add valuable redundancy at minimum cost [1].

Many strategies for nonintrusive monitoring have been developed over the last 20 years [2]–[7], [11]. Loads that draw varying power during operation tend to confound these methods. Variable-speed drives (VSDs) are one class of variable loads increasingly widely found in industrial and commercial facilities. The net energy consumption of a VSD cannot be computed by assuming a constant power consumption over a time interval bounded by turn-on and turn-off transients. The time-varying nature of VSD power demand also interferes with the load state estimator in a NILM, making it difficult even to keep track of the ON/OFF status of other nonvariable (constant) loads [11], [12].

The current supplied to a VSD typically exhibits distinct correlations between its fundamental and higher harmonic components. Other power electronic or nonlinear electromechanical loads with variable demands may also exhibit such harmonic signatures. This paper presents a technique of using unique harmonic signatures to monitor VSDs. This technique could be extended to any variable load with distinctive harmonic correlations.

The goal of this paper is to develop a VSD power estimation method based on correlations between fundamental and higher harmonic content. The power consumed by a VSD is estimated from observations of its higher harmonic current. The estimated VSD power can be subtracted from the aggregate power signal. When the colored noise associated with a VSD is also filtered, the remaining signal can be analyzed by a load-state estimator, to track the operations of *two state* or ON/OFF loads. Section II of this article reviews typical VSD construction and develops a correlation model. Section III introduces a method for estimating VSD power consumption. This method employs mean estimation, correlation mapping, and white filtering. The VSD power estimator is tested in Section IV with the power signal collected from a commercial building electric system. Section V summarizes the approach.

II. VSD Power Signal Model

Variable-speed drives are widely employed for energy efficiency or where a limited selection of speeds cannot meet demands. Machine tools, fans, pumps, and chillers are typical applications of VSDs. A VSD typically consists of a rectifier, a dc bus, and an inverter [13]. Fig. 1 shows the topology of a VSD, along with a typical circuit model. The rectifier converts three-phase ac currents to dc. The dc bus voltage is inverted to ac waveforms. The output frequency is adjusted by controlling the inverter timing.

The rectifier typically consists of a three-phase bridge with six diodes, delta connected to the utility [14] as shown in Fig. 1. The dc link voltage is filtered by a capacitor or *LC* filter before being fed to the inverter. Inductors can be placed between the supply

Manuscript received May 11, 2004; revised July 13, 2004. This work was supported by the California Energy Commission under Contract 400-99-011 and by Grainger Foundation. Paper no. TEC-00130-2004

K. D. Lee is with Applied Materials, Santa Clara, CA 95054 USA (e-mail: douglee@alum.mit.edu).

S. B. Leeb is with the Department of Electrical Engineering and Computer Science, Massachusetts Institute of Technology (MIT) (e-mail: sbleeb@mit.edu).

L. K. Norford is with the Department of Architecture, MIT (e-mail: lnorford@mit.edu).

P. R. Armstrong is with the Pacific Northwest National Laboratory (e-mail: peter.armstrong@pnl. gov).

J. Holloway is with the Department of Electrical Engineering and Computer Science, Massachusetts Institute of Technology Cambridge, MA (email: holloway@alum. mit.edu).

S. R. Shaw is with the Electrical and Computer Engineering Department, Montana State University (e-mail: sshaw@matrix.coe.montana.edu).

Digital Object Identifier 10.1109/TEC.2005.852963

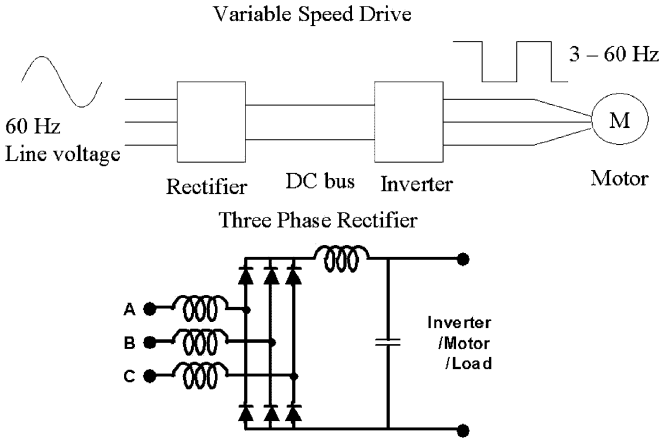

Fig. 1. Topology and typical circuit model of variable-speed drive.

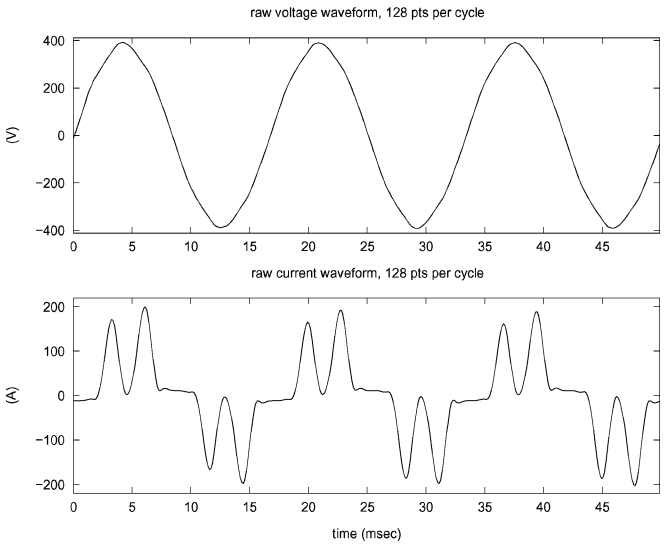

Fig. 2. Voltage and current waveforms of a VSD.

lines and the diodes to suppress the propagation of harmonics back to transmission lines. A phase current typically shows four peaks—two in a positive swing and two in a negative swing—in a single line cycle [3], [15].

Fig. 2 shows a representative VSD current waveform (phase A current, i_a), collected from a test building in San Francisco, CA. The figure clearly shows four peaks per cycle. For reference, the phase A line-to-neutral voltage is also shown. When the current waveform is multiplied by the peak voltage magnitude, V, it can be approximated by a (time-varying) Fourier series with following coefficients [2]:

$$P_k(t) = \frac{1}{T}\int_{t-T}^{t} i_a(s)V\cos\left(k\frac{2\pi}{T}(s)\right)ds \tag{1}$$

and

$$Q_k(t) = \frac{1}{T}\int_{t-T}^{t} i_a(s)V\sin\left(k\frac{2\pi}{T}(s)\right)ds \tag{2}$$

where the harmonic index k is a nonnegative integer and T is the period of the utility line cycle. For $k = 1$, the coefficients P_1

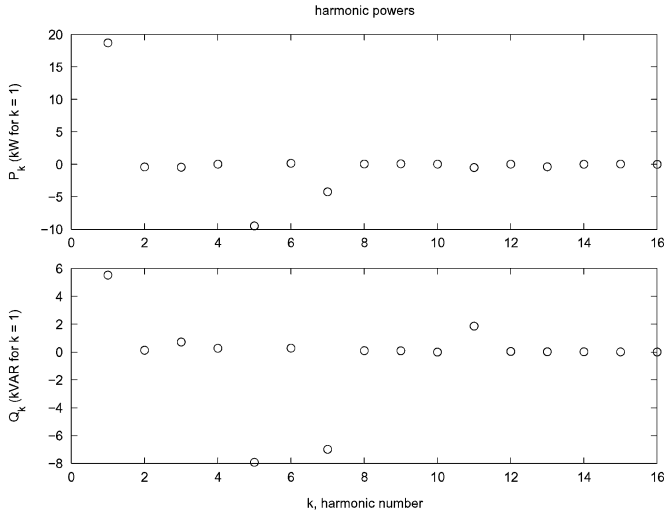

Fig. 3. Harmonic powers of a VSD (Fig. 2).

and Q_1 correspond to the conventional definitions of real and reactive phase power, respectively. For higher values of k, these harmonic *powers* or envelopes do not have widely recognized definitions and correspond simply to the harmonic content of the current waveform. Fig. 3 shows the harmonic powers computed from the waveforms in Fig. 2. The details of how to compute the harmonic powers from voltage and current waveform samples are discussed in [12]. A typical VSD draws significant quantities of P_1 (or P, real power), P_7, Q_1 (or Q, reactive power), Q_5, and Q_7.

Constant linear loads draw only P and Q, and do not generate higher harmonics. When a site contains only constant linear loads in addition to a VSD, selected higher harmonics can be used to keep track of the VSD fundamental powers. The method is applicable even when other nonlinear loads (e.g., single-phase rectifier) are present, if they do not generate harmonics monitored for the VSD tracking purpose. If other loads are present that also generate overlapping harmonics, it might still be possible to estimate the individual contributions from each load (type) by decomposing the observed power vector (with harmonic dimension), using orthogonal basis vectors associated with each load (type) [16].

Fig. 4 shows the time graphs of VSD harmonic powers, collected from the test building. The building has two VSDs that drive a supply fan (100 hp) and a return fan (75 hp) for air circulation. These fans are turned on and off at the same time and connected via an air duct system. They can be treated as a single unit for load tracking, because they operate in tandem and serve the same physical system. The VSDs turn on just before hour 7.8 in the plot.

Fig. 4 suggests strong correlations between the fundamental and higher harmonic powers. As P and Q rise, the magnitudes of fifth and seventh harmonic also rise. The third harmonic powers are essentially zero, though their noise variances increase with the magnitudes of the fundamental powers.

The steady-state power signal of a constant load can be modeled as a Gaussian random process [11], [12].

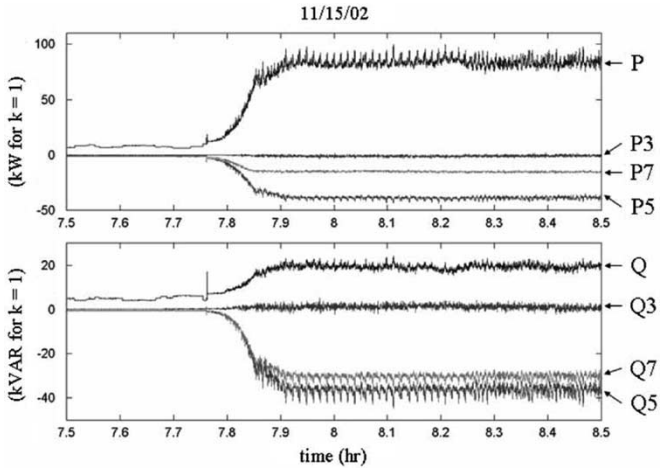

Fig. 4. Harmonic powers consumed by a pair of VSDs.

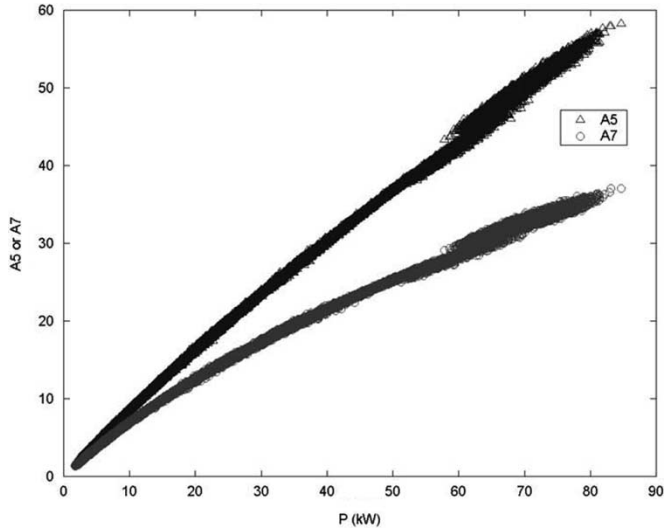

Fig. 5. Correlation graphs between real power and selected apparent powers.

Likewise, a VSD load vector $\mathbf{s}_i[n]$ can be modeled as Gaussian, i.e., $\mathbf{s}_i[n] \sim \mathcal{N}(\boldsymbol{\mu}_i[n], \boldsymbol{\Lambda}_i[n])$. The load vector $\mathbf{s}_i[n] = [P[n]\ Q[n]\ P_3[n]\ Q_3[n]\ P_5[n] \ldots]^T$ is the harmonic power vector at discrete time n consumed by load i. A constant load has a constant mean vector and a constant covariance matrix, whereas the mean and covariance of a VSD vary. We can introduce a simple model to account for their time-varying nature that is helpful for load tracking.

In estimating the mean vector, we assume that there exist certain relations among its components, i.e.,

$$\boldsymbol{\mu}_{i,j}[n] = f\left(\boldsymbol{\mu}_{i,1}[n], \ldots, \boldsymbol{\mu}_{i,j-1}[n], \boldsymbol{\mu}_{i,j+1}[n], \ldots\right) \quad (3)$$

where $\boldsymbol{\mu}_{i,1}[n]$ is the first component (real power) and $\boldsymbol{\mu}_{i,j}[n]$ is the jth component of the mean vector at time n. For a VSD, this function may be derived analytically, given the precise VSD circuit schematic, control scheme, and mechanical loading conditions. In practice, it is observed that a higher harmonic mean can be faithfully described by either the real or reactive mean

$$\boldsymbol{\mu}_{i,j}[n] \approx f(\boldsymbol{\mu}_{i,1}[n]) \approx g(\boldsymbol{\mu}_{i,2}[n]) \quad j \geq 5. \quad (4)$$

If the above functional relationships are one-to-one, the real and reactive means can be estimated from the measurement of a selected $\boldsymbol{\mu}_{i,j}[n]$, using inverse functions.

The covariance matrix is assumed to be proportional to the square of mean real power

$$\boldsymbol{\Lambda}_i[n] \approx \left(\frac{\boldsymbol{\mu}_{i,1}[n]}{\boldsymbol{\mu}_{i,1}[n_r]}\right)^2 \boldsymbol{\Lambda}_i[n_r] \quad (5)$$

where $\boldsymbol{\mu}_{i,1}[n_r]$ and $\boldsymbol{\Lambda}_i[n_r]$ are reference mean real power and covariance matrix taken at time n_r, respectively. In this way, the VSD load vector $\mathbf{s}_i[n]$ is statistically characterized, at least for the components with $k = 1$, when its fundamental means are estimated from the correlations of higher harmonic means.

Slight time shifts in samples of the voltage waveform can lead to a bias in the relative distribution of P_k and Q_k and the amount of bias increases with k [12]. To solve this problem, we can either construct a highly accurate harmonic envelope preprocessor or select an unbiased measure. One such measure is the kth apparent power or envelope A_k

$$A_k = \sqrt{P_k^2 + Q_k^2}. \quad (6)$$

The kth apparent power is simply the magnitude of the kth complex power, whose real part is the kth real power and imaginary part is the kth reactive power. The first apparent power A_1 has units of (VA). Because A_k is the magnitude of the discrete Fourier transform of the current waveform (with scale factor V), it is free from the bias created by time-shifted voltage samples [12].

Fig. 5 shows the correlation graphs between the real power and the fifth and seventh apparent powers. The data were collected at the test building. The graphs clearly show positive relationships between the real power and the fifth and seventh apparent powers. The relationships are not linear and the slopes decrease with increasing P. The correlation graph between Q and A_5 or A_7 showed a similar relationship. Also, the correlation graphs of VSDs collected from other sites showed comparable trends.

The correlation parameters exhibit small temporal variations, for a variety of reasons such as utility voltage waveform distortion and different electrical and mechanical loading conditions for VSDs. Empirically, the variations were typically 5% to 10%. This time-dependence can be observed in Fig. 5. The first two-thirds of the graphs were obtained by ramping up the VSDs for a short period of time. The rest, i.e., where $P \geq 60$ kW, were obtained by running the VSDs at their nominal operating points for a day. Slight loading condition changes on that day introduced scattering and minute shifts in the graphs. Ideally, it is desired to have a set of correlations and to choose the most likely correlation based on observations. However, in this paper, we use a single representative correlation to prove the concept.

Any reasonable curve fit of the correlation data can be used to map an apparent harmonic power to P (or Q) and vice versa. A piecewise power function model was convenient given our field data. For simplicity, we denote the kth apparent, real and

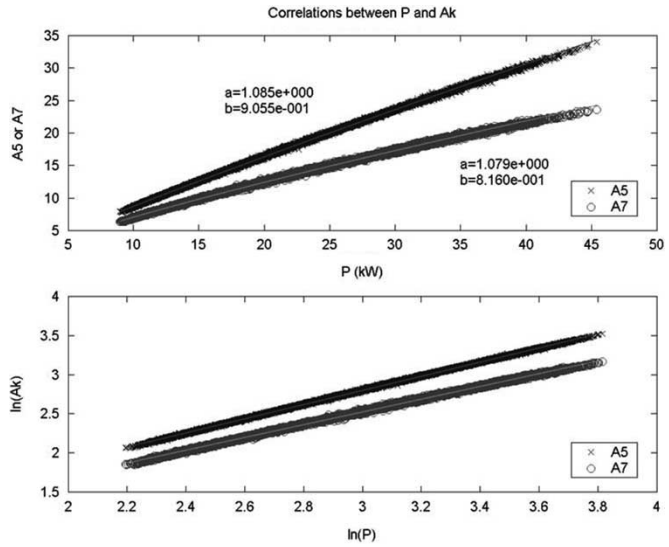

Fig. 6. Parameter estimation for one of the regions shown in Fig. 5.

reactive mean power as A_k, P_k, and Q_k, respectively. Consider a correlation between P and A_k for a given region. Then, A_k can be represented as a power function of P

$$A_k = f(P) = aP^b. \tag{7}$$

Taking the logarithm produces a linear function

$$\ln A_k = \ln a + b \ln P. \tag{8}$$

The parameters $\ln a$ and b can be estimated with the conventional method of least-squares (LS) for a given finite length observation. Fig. 6 shows the parameter estimation result for a region in Fig. 5. Resulting parameterized correlations are shown in solid lines along with the estimated parameters. The lower graph is in a logarithmic scale and the data points are almost perfectly linear. The procedure can be repeated for different regions to obtain a piecewise continuous correlation curve between A_k and P over the whole range. The correlation is one-to-one and thus invertible. The correlation between A_k and Q is also obtained in this manner.

III. VSD Power Estimation Method

This section develops a systematic methodology to estimate VSD power and to condition the fundamental aggregate powers for further load-status analysis. The overall signal processing schematic is shown in Fig. 7. The mean of a selected higher harmonic apparent power is first estimated. Given this mean, the correlation look-up table produces estimates of the VSD mean fundamental powers. These estimates are subtracted from the observations of P and Q. The remaining signals go through whitening filters, to remove colored noise generated by VSDs. However, any white noise added by a VSD is retained. Once the VSD power consumption and colored noise are removed, the load status analyzer can identify the operating status of other constant loads by detecting and classifying load (ON/OFF) events. Removing colored noise is essential for the load status analyzer that relies on the white Gaussian load model [12].

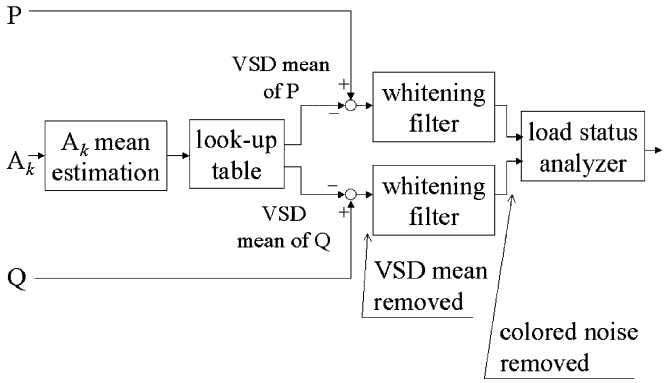

Fig. 7. Schematic of VSD power estimation and signal conditioning.

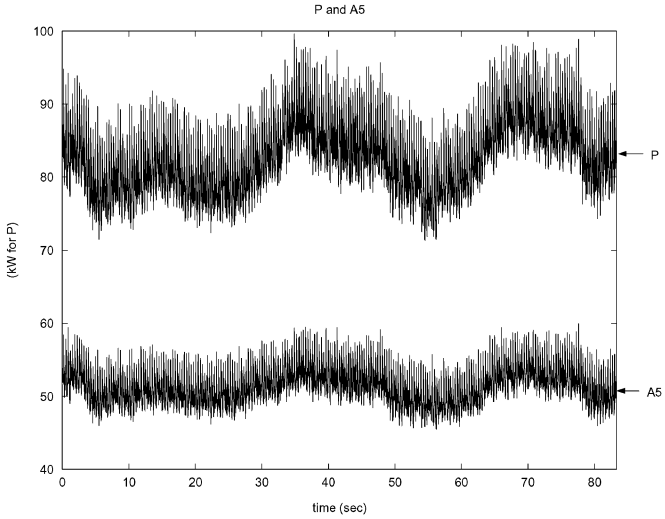

Fig. 8. Time graphs of P and A_5.

More than one apparent power could be used to estimate the fundamental powers consumed by a VSD. For example, we could use both A_5 and A_7 to estimate fundamental powers separately and take averages to obtain final estimation results. Here, we use only A_5 to demonstrate the approach.

The scheme is performed for a window of data to estimate the mean of A_k. The window size and the mean estimation method for A_k are determined by the nature of the signal. Fig. 8 shows the time graphs of P and A_5, collected at 120 Hz from the test building on 12/04/02. The graphs show the undulating nature of P, which is reflected in A_5. This slow oscillation is related to the nature of the air-handling system and how it is controlled [12].

Estimating the mean of A_5 as a sinusoidal function is difficult due to its time-varying nature. An alternative is to select a small size window and assume that the mean is described by a polynomial function of time indices. In this paper, we select the polynomial of order one (line). A first-order polynomial mean estimator is described in the Appendix.

Fig. 9 shows a detailed view of P and A_5 with window size $N = 256$, taken at $t = 58.3$ from Fig. 8. The bottom picture also shows the result of the first-order mean estimation as the dashed line. The appropriate A_5 mean estimation method and window size have been determined based on the observations.

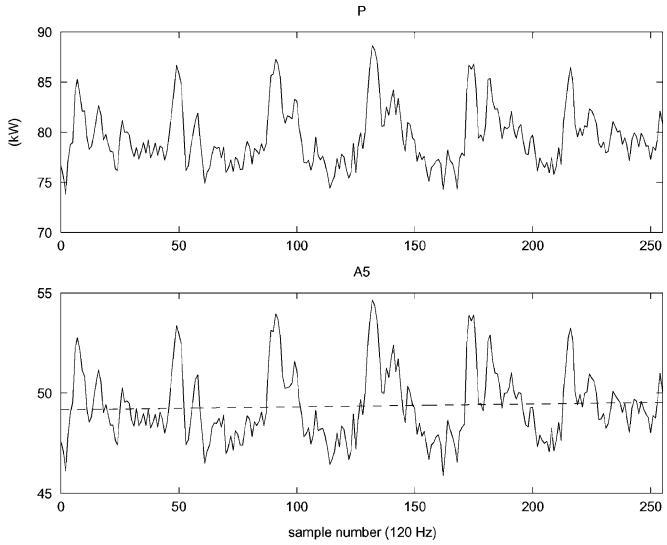

Fig. 9. Detailed view of P and A_5.

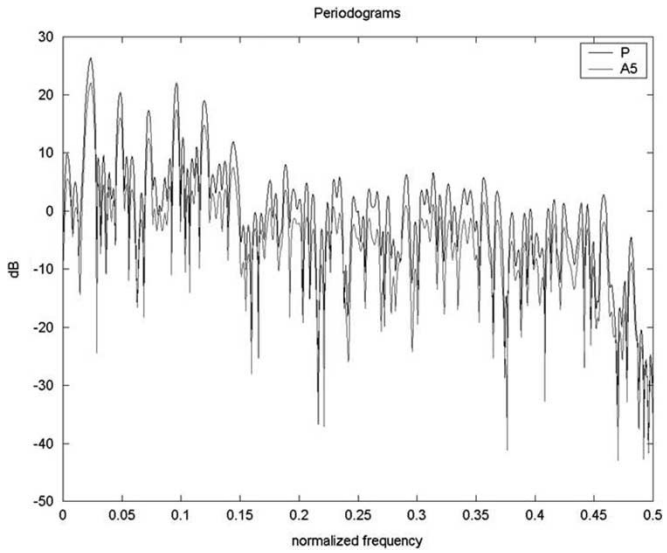

Fig. 10. Periodograms of signals in Fig. 9.

The peaks of P and A_5 are in phase and exhibit the same period ($\sim$3 Hz).

Fig. 10 shows the periodograms of the Fig. 9 signals. The frequency is normalized so that the unit normalized frequency is equal to the sampling frequency (120 Hz). Both periodograms show large spectral peaks at low frequencies, at the same locations. The peak heights of P and A_5 differ by a constant amount in a logarithmic scale. We may conclude that P and A_5 have almost identical noise spectral distributions, but differ in magnitudes by a constant scaling factor. This observation permits the construction of the whitening filter of P based on the spectral information of A_5 and vice versa.

Spectral components that are not integer multiples of the voltage frequency, e.g., 60 Hz, are sometimes called interharmonics [17]. Interharmonics are typically caused by either a periodically varying load or a frequency difference between two ac systems connected by a dc link [18]. A variety of mechanical conditions can present an unsteady load to a motor. Impeller imbalance, an off-center sheave, a bent shaft, and belt imperfections all can result in measurable periodic load components, for example. We will refer to these and similar conditions as a "load imbalance." In a VSD, interharmonics can be caused either by a load imbalance or by a dc ripple due to the frequency mismatch between rectifier and inverter. The interharmonics of the test building appear to be caused by a load imbalance, because their fundamental frequency is directly proportional to the VSD shaft rotation frequency [12]. We also note that the interharmonics, or colored noise, have a harmonic nature, i.e., their spectral locations are integer multiples of a frequency ($\sim$3 Hz).

If the colored noise is generated by a load imbalance, its magnitude can be used as a diagnostic indication of imbalance severity. Also, we can monitor the rotational speed of the fan by estimating the fundamental frequency of the harmonic noise. In other words, we can have a *virtual tachometer*. This observation has served as the basis for a number of motor speed and parameter estimation schemes in the literature [19]–[21].

To eliminate the colored noise generated by a VSD, we can either estimate the noise and subtract it from the observation or construct a filter. The former approach is useful when we are interested in estimating the harmonic noise for diagnosis and speed monitoring. The construction of an optimal whitening filter is closely related to the estimation of the power spectral density (PSD) of the signal. This paper uses the second approach, described in [12].

IV. Tests

The overall VSD mean power estimation scheme was tested for a span of data, collected at 120 Hz, from the test building on 12/04/02. The span consists of 30 nonoverlapping rectangular windows, each with $N = 256$ samples.

Fig. 11 shows the time waveform of A_5 and the first-order mean estimation of A_5 as the solid line. Because the mean estimation is linear piecewise continuous, it is not as smooth as the natural undulation of A_5, but follows reasonably well.

The upper graph in Fig. 12 shows the time waveform of P. The solid line is the VSD P mean estimation from the A_5 mean estimation via the correlation look-up table. The lower graph shows P after its VSD mean is subtracted and white-filtered. The remaining activity in the difference signal is due in part to the activity of small ON/OFF (background) loads in the building, and to the minute time-varying nature of mean power correlations. The VSD mean estimation and white-filtering of Q showed similar results.

Fig. 13 shows the standard deviations of the white filtered signals. Fig. 14 shows the periodograms of P and Q before and after white filtering for a window of data. Large spectral peaks have disappeared after filtering, and the periodograms are relatively flat for the overall frequency range, implying the effectiveness of the white filtering.

A real-time, Web-based VSD power estimator (VSD tracker) was developed and installed at the test building [12]. Fig. 15 shows its history page (past 9 h). The display samples are taken

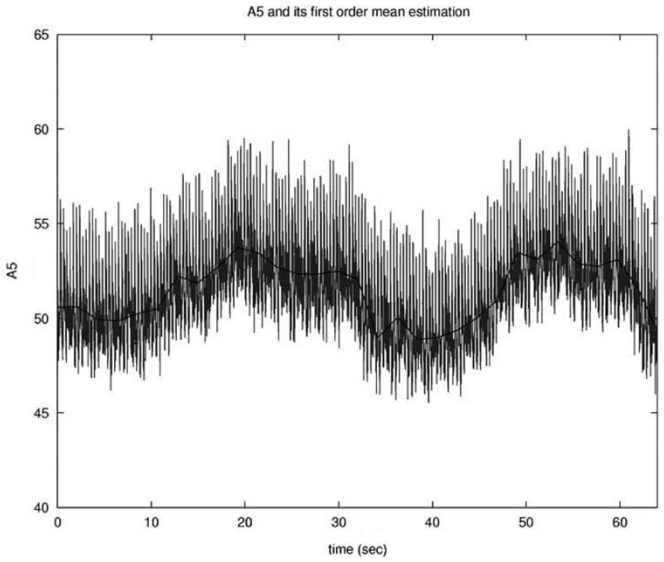

Fig. 11. A_5 with its first-order mean estimation and innovations.

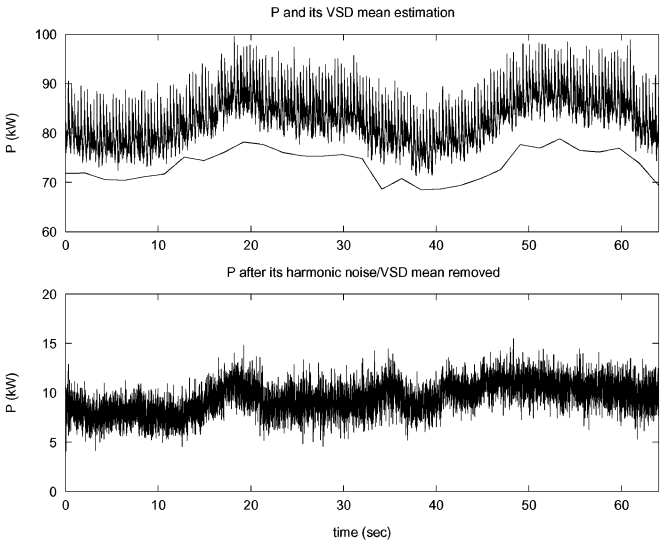

Fig. 12. P with its VSD mean estimation and innovations.

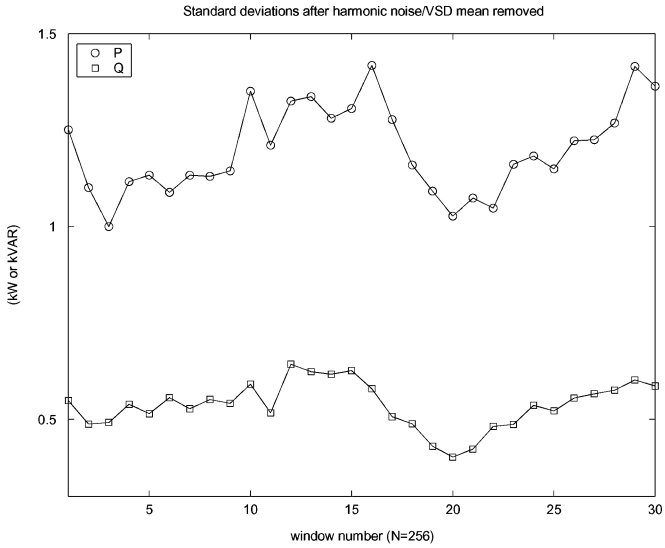

Fig. 13. Standard deviations of innovations at each window.

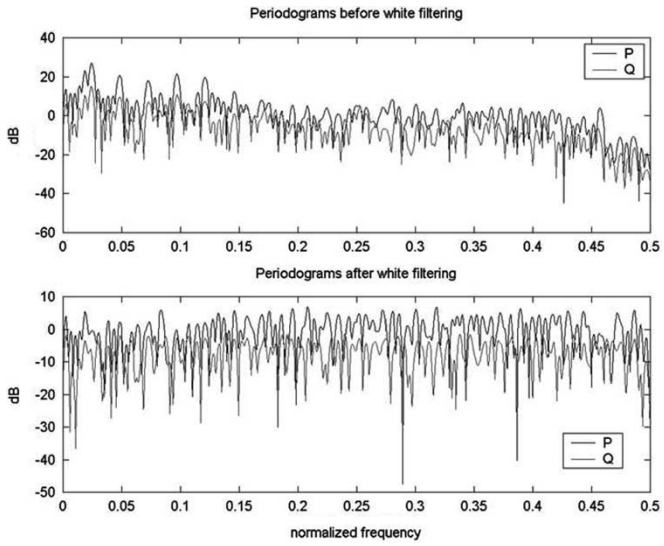

Fig. 14. Periodograms of P and Q before and after white filtering.

every 1 min and are averages of 1024 original (120-Hz) samples. The fifth apparent power is almost constant. The graphs show that there was a constant load activity, evidenced by the step changes in the real and reactive power waveforms. However, because the fifth apparent power was unaffected, the VSD fundamental power estimations were still successful. The step changes are conserved in the differences or non-VSD power signals. This example clearly shows that the VSD tracker can disaggregate total powers into the powers consumed by VSDs and non-VSD loads. A conventional NILM algorithm can then identify and track the activity of constant loads in the difference stream.

V. Summary

The power estimation technique presented in this paper extends the applicability of the nonintrusive load monitoring approach to environments that include loads with continuously varying power consumption. Any continuously variable load that generates a unique higher harmonic signature can be disaggregated, in principle, using the methods developed in this paper. The method could conceivably be extended to situations in which several different varying loads are present, provided that each presents a unique harmonic pattern.

This paper introduced a Gaussian random process model for a VSD, with time-varying mean and covariance. The model was simplified by assuming that there exist strong correlations between mean harmonic powers. The one-to-one relationship between a higher harmonic mean and a fundamental mean was modeled by the piecewise power function and used to estimate VSD fundamental powers from the estimation of a higher harmonic mean. The colored noise generated by a VSD was removed by a whitening filter and the difference signal could be examined by the load status analyzer.

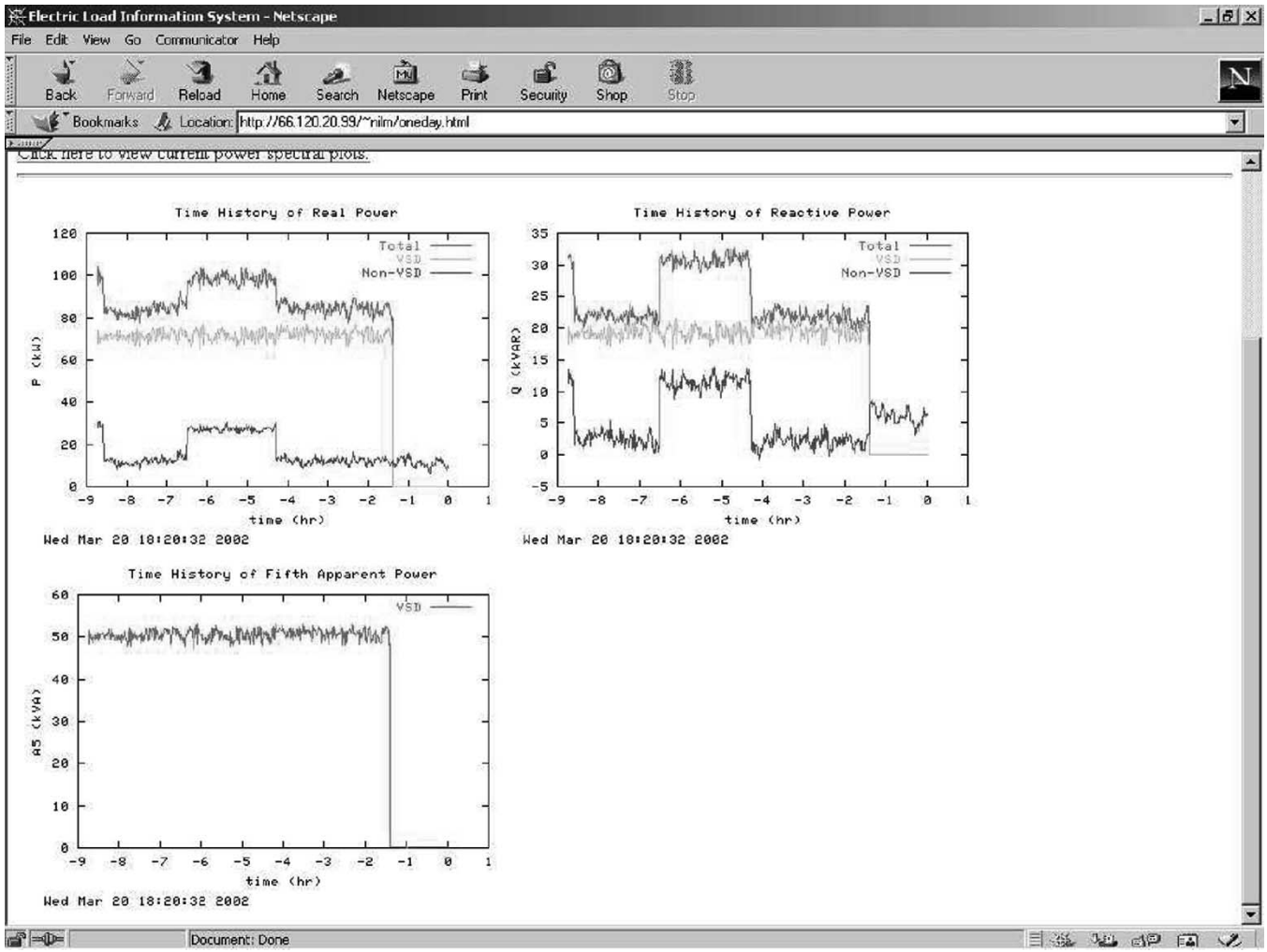

Fig. 15. VSD tracker history page (21:27 4/3 2003 EST).

Test results show the effectiveness of the VSD power estimation method. The method could also be enhanced with more sophisticated correlating functions relating higher harmonic content to fundamental powers. As presented, the disaggregation scheme developed here has enabled real-time, Web-based monitoring of the activity of both VSDs and constant loads in a test building.

APPENDIX

This appendix develops a first-order polynomial mean estimator to represent the time-varying mean of a random process as a succession of first-order polynomials. The random process is first modeled as white Gaussian and the maximum-likelihood (ML) estimator is derived. It is shown that the least-squares error criterion leads to the same formula and that the ML estimator can be used for non-Gaussian additive noise in a least-squared error sense.

Suppose that $\mathbf{x}$ is a length-N observation of a random process, e.g., an apparent power A_k,

$$\mathbf{x} = [x[0]\ x[1]\ \ldots\ x[N-1]]^T. \tag{9}$$

We assume that $x[n]$ is the sum of a first-order polynomial mean and a white noise

$$x[n] = m_x[n] + w[n] \quad 0 \le n \le N-1 \tag{10}$$

where $m_x[n] = \alpha n + \beta$ and $\mathrm{var}(w[n]) = \sigma^2$. With this signal model, the observation vector $\mathbf{x}$ follows a Gaussian distribution with the probability density function (PDF)

$$p(\mathbf{x}\,|\,\alpha,\beta) = \frac{\exp\left(-\frac{1}{2}(\mathbf{x}-\mathbf{m}_\mathbf{x})^T\mathbf{\Lambda}_\mathbf{x}^{-1}(\mathbf{x}-\mathbf{m}_\mathbf{x})\right)}{(2\pi)^{\frac{N}{2}}\det^{\frac{1}{2}}(\mathbf{\Lambda}_\mathbf{x})} = \frac{\exp\left(-\frac{1}{2\sigma^2}\sum_{n=0}^{N-1}(x[n]-\alpha n-\beta)^2\right)}{(2\pi)^{\frac{N}{2}}\sigma^N} \tag{11}$$

where α and β are the parameters of the distribution.

The maximum likelihood estimations of these parameters are found by maximizing the logarithm of the PDF with respect to α and β. The maximums logarithm of the PDF is a quadratic function of α and β, the maximums occur where the first derivatives

are zero

$$\frac{\partial \ln p(\mathbf{x}\,|\,\alpha,\beta)}{\partial \alpha} = \frac{1}{\sigma^2}\sum_{n=0}^{N-1} n(x[n]-\alpha n-\beta) = 0$$

$$\frac{\partial \ln p(\mathbf{x}\,|\,\alpha,\beta)}{\partial \beta} = \frac{1}{\sigma^2}\sum_{n=0}^{N-1} (x[n]-\alpha n-\beta) = 0. \quad (12)$$

By combining these two equations, we obtain the following single matrix equation:

$$\mathbf{A}\mathbf{a} = \mathbf{b} \quad (13)$$

where

$$\mathbf{A} = \begin{bmatrix} \sum_{n=0}^{N-1} n^2 & \sum_{n=0}^{N-1} n \\ \sum_{n=0}^{N-1} n & \sum_{n=0}^{N-1} 1 \end{bmatrix} = \begin{bmatrix} \frac{N(N-1)(2N-1)}{6} & \frac{N(N-1)}{2} \\ \frac{N(N-1)}{2} & N \end{bmatrix}$$

$$\mathbf{a} = [\alpha \quad \beta]^T \quad \text{and} \quad \mathbf{b} = \begin{bmatrix} \sum_{n=0}^{N-1} nx[n] & \sum_{n=0}^{N-1} x[n] \end{bmatrix}^T. \quad (14)$$

The matrix $\mathbf{A}$ is a function of N only and invertible whenever $N \geq 2$.

The same formula can be derived by using the least-squares (LS) error criterion, i.e.,

$$\mathbf{x} \approx \alpha\mathbf{n} + \beta\mathbf{1} = \mathbf{H}\mathbf{a} \quad (15)$$

where $\mathbf{H} = [\mathbf{n}\ \mathbf{1}]$ and $\mathbf{n} = [0\ 1\ \cdots\ N-1]^T$. The LS estimation of $\mathbf{a}$ is given by

$$\hat{\mathbf{a}} = (\mathbf{H}^T\mathbf{H})^{-1}\mathbf{H}^T\mathbf{x}. \quad (16)$$

Readers can easily verify that $\mathbf{H}^T\mathbf{H} = \mathbf{A}$ and $\mathbf{H}^T\mathbf{x} = \mathbf{b}$.

Thus, when the additive noise is white Gaussian, we have an ML first-order polynomial mean estimator, which is approximately a minimum variance unbiased estimator [23]. When the noise is not white, the same mean estimator is still valid in the LS error sense. The latter viewpoint is especially helpful because power signals typically carry colored noise.

When the first-order mean estimation is performed on a series of windows, we may impose an additional constraint that the mean estimation is continuous across windows. Suppose that $\mathbf{m}_{\mathbf{x},j}$ is the length-N mean vector of the jth window and that $\mathbf{m}_{\mathbf{x},j-1}$ is the length-N mean vector of the preceding $(j-1)$th window. The constraint can be stated as $m_{x,j-1}[N] = m_{x,j}[0]$, or

$$\alpha_{j-1}N + \beta_{j-1} = \beta_j. \quad (17)$$

Thus, with the continuity constraint, the parameter β of a current window is determined solely by the parameters of its preceding window. The remaining parameter α_j is obtained by solving the first derivative condition:

$$\alpha_j = \frac{\sum_{n=0}^{N-1} nx[n] - \beta_j \sum_{n=0}^{N-1} n}{\sum_{n=0}^{N-1} n^2} = \frac{\sum_{n=0}^{N-1} nx[n] - \beta_j \frac{N(N-1)}{2}}{\frac{N(N-1)(2N-1)}{6}}. \quad (18)$$

REFERENCES

[1] C. Laughman, K. D. Lee, R. Cox, S. Shaw, S. B. Leeb, L. K. Norford, and P. Armstrong, "Advanced nonintrusive monitoring of electric loads," *IEEE Power Energy Mag.*, vol. 1, no. 2, pp. 56–63, Mar./Apr. 2003.

[2] S. B. Leeb, S. R. Shaw, and J. L. Kirtley Jr., "Transient event detection in spectral envelope estimates for nonintrusive load monitoring," *IEEE Trans. Power Del.*, vol. 10, no. 3, pp. 1200–1210, Jul. 1995.

[3] S. R. Shaw, C. B. Abler, R. F. Lepard, D. Luo, S. B. Leeb, and L. K. Norford, "Instrumentation for high performance nonintrusive electrical load monitoring," *ASME J. Solar Energy Eng.*, vol. 120, no. 3, pp. 224–229, Aug. 1998.

[4] F. Sultanem, "Using appliance signatures for monitoring residential loads at meter panel level," *IEEE Trans. Power Del.*, vol. 6, no. 4, pp. 1380–1385, Oct. 1991.

[5] S. B. Leeb and J. L. Kirtley Jr., "Transient event detector for use in nonintrusive load monitoring systems," U.S. Patent 5 483 153, Jan. 9, 1996.

[6] M. Tubaishat and S. Madria, "Sensor networks: An overview," *IEEE Potentials*, vol. 22, no. 2, pp. 20–23, Apr./May 2003.

[7] L. Carmichael, "Nonintrusive appliance load monitoring system," *EPRI J. Elect. Power Res. Inst.*, pp. 45–47, Sep. 1990.

[8] A. I. Cole and A. Albicki, "Algorithm for non-intrusive identification of residential appliances," in *Proc. IEEE Int. Symp. Circuits and Systems (ISCAS)*, vol. 3, 1998, pp. 338–341.

[9] S. Drenker and A. Kader, "Nonintrusive monitoring of electric loads," *IEEE Comput. Appl. Power*, vol. 12, no. 4, pp. 47–51, Oct. 1999.

[10] G. W. Hart, "Nonintrusive appliance load monitoring," *Proc. IEEE*, vol. 80, no. 12, pp. 1870–1891, Dec. 1992.

[11] K. D. Lee, S. B. Leeb, and L. K. Norford, "Constant electric load state estimation via load event identification,", to be submitted to the IEEE Transactions on Energy Conversion.

[12] K. D. Lee, "Electric load information system based on non-intrusive power monitoring," Ph.D. dissertation, Mass. Inst. Tech. Dep. Mech. Eng., 2003.

[13] B. K. Bose, "Variable frequency drives-technology and applications," in *Proc. IEEE Int. Symp. Industrial Electronics, ISIE93*, Budapest, Hungary, 1993, pp. 1–18.

[14] C. W. Lander, *Power Electronics*, 2nd ed., New York: McGraw-Hill, 1987.

[15] W. Xu, H. W. Dommel, M. B. Hughes, G. W. K. Chang, and L. Tang, "Modeling of adjustable speed drives for power system harmonic analysis," *IEEE Trans. Power Del.*, vol. 14, no. 2, pp. 595–601, Apr. 1999.

[16] S. B. Leeb, B. C. Lesieutre, and S. R. Shaw, "Determination of load composition using spectral envelope estimates," in *Proc. 27th Annu. North American Power Symp.*, Bozeman, MT, Oct. 1995, pp. 618–627.

[17] R. Yacamini, "Power system harmonics, part 4: Interharmonics," *IEE Power Eng. J.*, pp. 185–193, Aug. 1996.

[18] C. Li, W. Xu, and T. Tayjasanant, "Interharmonics: Basic concepts and techniques for their detection and measurement," Unpublished.

[19] K. D. Hurst and T. G. Habetler, "A comparison of spectrum estimation techniques for sensorless speed detection in induction machines," *IEEE Trans. Ind. Appl.*, vol. 33, pp. 898–905, Jul./Aug. 1997.

[20] P. Vas, *Sensorless Vector and Direct Torque Control*. Oxford, U.K.: Oxford Univ. Press, 1998.

[21] J. Nash, "Direct torque control induction motor vector control without an encoder," *IEEE Trans. Ind. Appl.*, vol. 33, pp. 333–341, Mar./Apr. 1997.

[22] J. G. Proakis, C. M. Rader, F. Ling, C. L. Nikias, M. Moonen, and I. K. Proudler, *Algorithms for Statistical Signal Processing*. Upper Saddle River, NJ: Prentice-Hall, 2002.

[23] S. M. Kay, *Fundamentals of Statistical Signal Processing, Volume I: Estimation Theory*. Englewood Cliffs, NJ: Prentice-Hall, 1993.

Kwangduk Douglas Lee received the B.S. degree from Pohang University of Science and Technology, Pohang, Korea in 1998, and the S.M. and Ph.D. degrees from the Massachusetts Institute of Technology (MIT), Cambridge, MA, in 2000 and 2003, respectively, all in mechanical engineering.

His research interests include signal processing and control, and their applications to engineering systems. He is currently a Process Engineer at Applied Materials.

Steven B. Leeb (SM'01) received the S.B., S.M., E.E. and Ph.D. degrees from the Massachusetts Institute of Technology (MIT), Cambridge.

He has been a member of the MIT faculty in the Department of Electrical Engineering and Computer Science since 1993. He serves as an Associate Professor in the Laboratory for Electromagnetic and Electronic Systems. He is concerned with the design, analysis, development and maintenance process for all kinds of machinery with electrical actuators, sensors or power-electronic drives.

Leslie K. Norford received the Ph.D. degree in mechanical and aerospace engineering from Princeton University, Princeton, NJ.

He is a Professor of building technology in the Department of Architecture at the Massachusetts Institute of Technology, Cambridge, where he has been a member of the faculty since 1988. His research interests concern monitoring the performance of mechanical and electrical equipment in buildings, optimization techniques as applied to the design of buildings and their mechanical systems, simulation of the performance of building equipment and efforts in support of sustainable buildings in developing countries.

Peter R. Armstrong received the Ph.D. degree from the Massachusetts Institute of Technology, Cambridge, in 2004.

He is Senior Research Engineer at Pacific Northwest National Laboratory. His research interests include adaptive models for optimal control and fault detection in buildings and thermofluid processes and measurement and analysis techniques for estimating parameters in the lab and in the field.

Jack Holloway (S'04) is a graduate student in the Department of Electrical Engineering and Computer Science Department, Massachusetts Institute of Technology, Cambridge.

Steven R. Shaw (SM'05) received the S.B., M.Eng., E.E., and Ph.D. degrees from the Massachusetts Institute of Technology, Cambridge.

He is currently an Assistant Professor in the Department of Electrical and Computer Engineering at Montana State University, Bozeman. He is interested in sensors, instrumentation, modeling, and numerical and computational methods associated with control and measurement problems.